RSC Advances

Co-delivery of hesperetin enhanced bicalutamide induced apoptosis by exploiting mitochondrial membrane potential via polymeric nanoparticles in PC-3 cell line

Journal:	*RSC Advances*
Manuscript ID	RA-ART-11-2015-023067.R1
Article Type:	Paper
Date Submitted by the Author:	09-Dec-2015
Complete List of Authors:	Arya, Abhishek; Central Drug Research Institute (CDRI), Pharmaceutics Khandelwal, Kiran; Central Drug research Institute, Pharmaceutics Ahmad, Hafsa; CSIR-CDRI, Pharmaceutics Laxman, Tulsankar; Academy of Scientific and Innovative Research (AcSIR), Anusandhan Bhawan, Rafi Marg, ; CSIR-Central Drug Research Institute, Lucknow, Pharmacokinetics & Metabolism Div Sharma, Komal; Central Drug Research Institute (CDRI), Pharmaceutics MITTAPELLY, NARESH; CSIR-Central Drug Research Institute, Pharmaceutics agrawal, satish; Central Drug Research Institute (CDRI), Pharmaceutics BHATTA, RABI; CSIR-Central Drug Research Institute , Pharmacokinetics and Metabolism Dwivedi, Anil; Central Drug research Institute, Pharmaceutics
Subject area & keyword:	Nanomaterials - Nanoscience < Nanoscience

RSC Advances

ARTICLE

Co-delivery of hesperetin enhanced bicalutamide induced apoptosis by exploiting mitochondrial membrane potential via polymeric nanoparticles in PC-3 cell line

Received 00th January 20xx,
Accepted 00th January 20xx

DOI: 10.1039/x0xx00000x

www.rsc.org/

Abhishek Arya[a,b], Kiran Khandelwal[a,d], Hafsa Ahmad[a], Tulsankar Sachin Laxman[b,c], Komal Sharma[a,b], Naresh Mittapelly[a,b], Satish Agrawal[a,b], Rabi S. Bhatta[c], Anil K. Dwivedi[a]*

In this research, we reported co-delivery of anti-androgen drug Bicalutamide (BCT) with Hesperetin (HSP) in chitosan (CS) coated polycaprolactone (PCL) nanoparticles (NPs) to increase therapeutic efficacy against androgen independent prostate cancer cell line. The PCL-BCT-HSP-CS NPs were prepared by anti-solvent precipitation followed by ionic gelation method, which showed narrow particle size distribution, high encapsulation efficiency (about 90%) and sustained drug release behavior of both drugs. During the preparation of NPs; HSP crystallinity was retained, whereas polymorphic transition of BCT from form I to form II was observed by thermogravimetric analysis. Additionally, DPPH radical scavenging assay confirmed structural integrity of HSP in NPs. The kinetic solubility of BCT and HSP in NPs was increased by 61.66, 6.75 folds, respectively as compared to free drugs. Further, in vitro therapeutic efficacy of co-loaded PCL-BCT-HSP-CS NPs was compared with free BCT, HSP and their combination (BCT plus HSP) in androgen independent PC-3 cell lines. Interestingly, co-loaded NPs exhibited higher in vitro cytotoxicity by G1-S phase cell cycle arrest and apoptosis at equivalent concentrations. This superior activity may be attributed to enhanced mitochondrial membrane potential loss by co-loaded NPs. Cell uptake study showed significantly higher ($P < 0.05$) uptake of NPs by cancer cells. Additionally, in vivo pharmacokinetics of NPs were explored in SD male rats revealed high $AUC_{0\text{-}t}$ and C_{max} of BCT (1.46 and 1.42 fold) and HSP (4.16 and 3.79 fold) than aqueous suspension when administered orally at 20mg/kg. We demonstrated that co-delivery with HSP via polymeric NPs might have better therapeutic potential for *in vitro* management of androgen independent prostate cancer.

1. Introduction

Prostate cancer is the most common (after lung cancer) and prevailing cause of death in older men which are typically due to the complication aroused by its invasion in to bones and other tissues [1]. According to The American Cancer Society in 2015, about 220,800 new cases and 27,540 deaths were reported in United States [2]. Bicalutamide (BCT), an oral non-steroidal anti-androgen drug has been approved for treatment of androgen dependent prostate cancer [3]. Although BCT has an elimination half-life of 5-7 days, it is administered once daily (Casodex® 50mg/kg). Therefore, administration of BCT causes drug accumulation and toxicities [4]. However, long term treatment with BCT therapy instigates mutation in androgen receptors and it starts acting as receptor agonist which results in failure of anti-androgen therapy [5]. Over the past few years, combination therapy of anti-cancer drugs with anti-oxidants has been widely employed for their synergistic activity. Predominantly, combination therapy can enhance therapeutic efficiency, while reducing undesirable side effects [6-8].

Herein, we choose Hesperetin (HSP), a natural bioflavonoid with promising anti-cancer, anti-oxidant, anti-inflammatory and chemo-preventive properties for co-delivery [9]. Sambantham *et. al* reported that HSP induces apoptosis by down regulating anti-apoptotic gene BCL_{XL} and increase the expression of pro-apoptotic genes like *BAD* at mRNA level. It also reduce cellular proliferation in androgen independent PC-3 cancer cell lines [10]. The clinical use of BCT and HSP has been limited due to their low efficacy against androgen independent prostate cancer, water solubility and *in vivo* bioavailability. The poor bioavailability of hydrophobic drugs demands high dosage to overcome sub-therapeutic levels in plasma [11, 12]. For co-delivery of drugs, various delivery systems have been investigated like micelles [13], bio-conjugation [14], nanoparticles (NPs) [15] and liposomes [16]. Among these, biodegradable nanocarriers have immense potential to deliver two or more drugs. Co-delivery by a single nanocarrier ensures controlled drug ratios, same drug disposition behavior and thus maximizing therapeutic outcome. A study on therapeutic

[a] *Pharmaceutics Division, CSIR-Central Drug Research Institute, Lucknow-226031, INDIA*
[b] *Academy of Scientific & Innovative Research, Chennai-600113, INDIA*
[c] *Pharmacokinetics and Metabolism, CSIR-Central Drug Research Institute, Lucknow-226031, INDIA;*
[d] Jawaharlal Nehru University, *New Delhi-110067, INDIA*
[e] *† Footnotes relating to the title and/or authors should appear here.*
[f] *Electronic Supplementary Information (ESI) available: [details of any supplementary information available should be included here]. See DOI: 10.1039/x0xx00000x*

benefits of two different nanocarrier carrying Curcumin and a platinum drug revealed a less noticeable synergistic effect in comparison to their co-delivery in single carrier [17]. As one of the major mechanism to target cancer cells is induction of apoptosis by *intrinsic* mitochondrial pathways. During apoptosis, loss of mitochondrial membrane potential occurs for complete release of cytochrome c which ultimately leads to activation of apoptotic caspases [18]. Targeting of mitochondria by cancer therapeutics has gained considerable attention as it causes less damage to normal tissues [19].

The present work was undertaken for co-delivery of BCT and HSP by using polycaprolactone (PCL) and chitosan (CS) as drug delivery carrier for mitochondrial targeting. PCL is a well-known synthetic bioresorbable and biocompatible polymer widely used as a carrier for drug delivery. Because of its hydrophobicity and high crystallinity, it is chemically stable and undergoes very slow degradation by hydrolysis of ester linkage. Colloidal carriers based on PCL were mostly designed by emulsion solvent evaporation, salting out, nano-precipitation, spray drying, supercritical fluid technology and hot melt technique [20, 21]. In order to make mucoadhesive NPs, CS was used as a suitable biodegradable cationic polysaccharide. Recent studies performed by Shrestha N. et. al revealed 20 fold increase in the intestinal permeability of Insulin by CS decorated nanocarriers as compared to pure insulin [22]. Also Curcumin encapsulation in CS coated PCL NPs resulted in increased efficiency against metastasis in lungs cancer [23].

Consequently, polymeric NPs co-loaded with BCT and HSP were prepared to address complications due to low efficiency, low bioavailability and hydrophobicity. The goal of preparing co-loaded NPs was to enhance BCT efficacy against androgen independent prostate cancer with subsequent reduction in oxidative damage. Therefore, androgen independent PC-3 cell line was appropriately selected for in vitro activity assessment assays. We determined physiochemical properties, drug loading and release behavior of NPs, and evaluate in vitro activity against PC-3 cells to assess effect of co-delivery. Further, oral pharmacokinetics and drug disposition studies were performed in male Sprague-Dawley (SD) rats. It is projected that simultaneous delivery of both drugs in one carrier would lead to an effective strategy for *in vitro* management of androgen independent prostate cancer.

2. Discussion

The main purpose of present study is; (a) to increase therapeutic efficacy of BCT by co-delivery with anti-oxidant, and (b) to enhance oral bioavailability by means of increasing solubility; using nanocarrier based drug delivery system against androgen independent prostate cancer cell line. To accomplish aforesaid objectives, we hypothesized the preparation of PCL-BCT-HSP-CS NPs **(Figure 1A)** so that higher plasma levels of BCT will be available for pharmacological effect and HSP was incorporated in a perspective to escalate its efficacy.

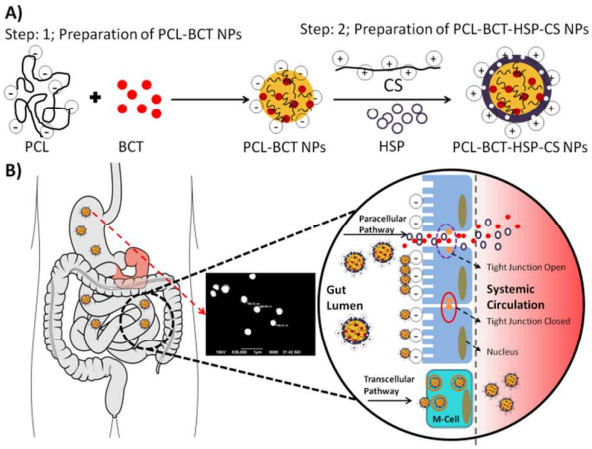

Figure 1A. Schematic representation of preparation of PCL-BCT-HSP-CS NPs, **(1B)** Representation of presumed mechanism of paracellular and transcellular transport of drugs from PCL-BCT-HSP-CS NPs from gut lumen to systemic circulation and its representative SEM image.

Biodegradable NPs are suitable drug delivery carrier for hydrophobic drugs with high loading efficiency and also possess ability to modulate pharmacokinetics. Moreover, drug encapsulation also prevents physical/chemical drug degradation and inactivation [24, 25].

For preparation of any drug delivery system, preliminary step is to evaluate compatibility of drug(s) with excipients. Here, we ensured the compatibility by Differential Scanning Calorimetry (DSC) analysis as endothermic peaks of BCT (194.10^{o}C) and HSP (226.24^{o}C) were retained in their physical combination with PCL and CS **(Figure 2A & 2B)**. It has been established that BCT exists in two polymorphic forms [26]. During the NPs processing, change in crystalline behavior of BCT was observed. To confirm this, TGA weight loss curve of BCT and plain precipitated BCT was compared **(Figure 2C)**. The decrease in temperature for maximum weight loss will be ascribed to formation of form II which posses different molecular conformation, crystal lattice and physiochemical properties. Whereas, crystallinity of HSP was retained in NPs. The surface morphology of BCT was modified while precipitation indicating the reformation in crystal lattice (formation of form II). Their SEM images has been shown in **Figure 2D**.

Particle size and zeta potential are important parameters for consideration in oral absorption, systemic distribution, toxicity and stability of NPs [27]. Therefore, type and concentration of surfactant was optimized carefully to achieve desirable particle size and zeta potential with narrow PDI. Four different surfactants such as pluronic F-127 (PF-127), polyvinyl alcohol (PVA), pluronic F-68 (PF-68) and Tween-80 (T-80) were evaluated for preparation of stable NPs. By increasing concentration of PF-127, PVA and PF-68 zeta potential decreased due to charge destabilization and hence, aggregation was induced. In contrast, T-80 resulted in increase in zeta potential that provides sufficient charge for electrostatic repulsion and prevented the aggregation of

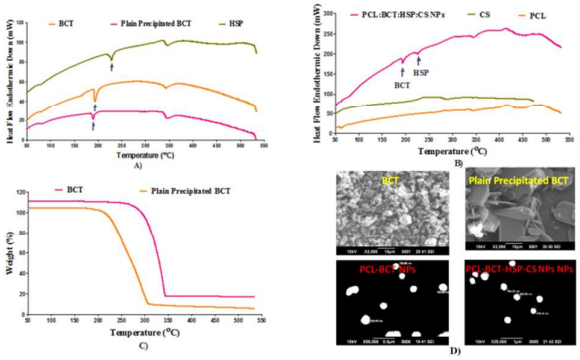

Figure 2A & 2B. Representation of DSC thermogram of BCT, HSP, plain precipitated BCT, PCL, CS and BCT+HSP+PCL+CS. **(2C)** TGA weight loss curve of BCT and plain precipitated BCT. **(2D)** SEM images of BCT, plain precipitated BCT, PCL-BCT NPs and PCL-BCT-HSP-CS NPs.

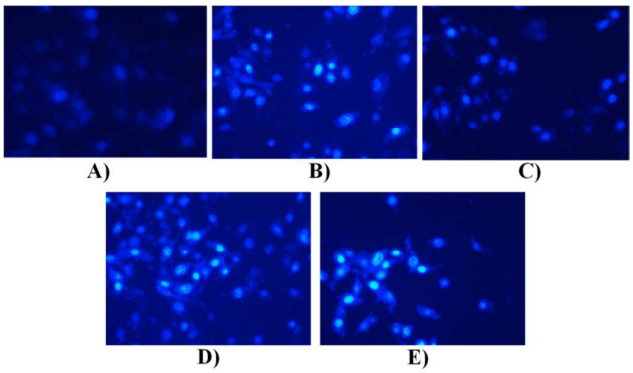

Figure 3. Fluorescent microscopic images of DAPI stained PC-3 cells after treatment with A) Blank NPs, B) BCT, C) HSP, D) BCT plus, and E) HSP PCL-BCT-HSP-CS NPs when treated with 100µM for 24hr. DAPI staining showed the number of apoptotic nuclei after each treatment.

particles and leads to reduction in particle size and narrower size distribution. Based upon the screening of surfactants; 0.25% v/v T-80 was found the most suitable surfactant as it imparted satisfactory diminution of interfacial tension and prevented aggregation of particles. Particle size obtained was 167±13.8nm having zeta-potential of -18.4±2.13mV which provide sufficient charge for electrostatic attraction to protonated CS. As a consequence of CS coating, particle size was increased to 281±15.2nm and zeta potential was changed to +12.10±1.20mV. NPs smaller than 300 nm are preferentially suitable for gastrointestinal uptake. Further positive surface is interesting characteristic as it imparts cell adhesion via interaction with the negatively charged sialic acid groups in mucin *in vivo*. SEM analysis showed size and surface morphology of PCL-BCT NPs and PCL-BCT-HSP-CS NPs **(Figure 2D)**. Huang P. et. al also reported change in zeta potential of PCL-grafted hyaluronic acid NPs by coating with CS, indicating the success of positively charged CS coating [28]. The prepared NPs were stable at refrigerated condition and it can be selected as suitable storage condition. We also studied effect of polymorphism on solubility of BCT. The plain precipitated BCT showed 3.6 times higher solubility than pure BCT which might be due to the formation of form II. Besides, NPs showed further increase in solubility (16.81 times) which may be due to combine effect of polymorphism and smaller particle size. Also, the solubility of HSP in NPs was increased by 6.75 times owing to particle size reduction which provides better surface area for dissolution.

Drug release from NPs was more sustained and continuously increasing throughout the study whereas aqueous suspension did not show notable release after 48hr. This might be imputed to the low aqueous solubility of BCT in aqueous suspension. Here, solubility of drug dominated over hydrophobicity of PCL core thereby percent drug released was increased over the time and sustained behavior was allied to the slow diffusion of drug into release media. As NPs did not show initial burst release which confirmed unbound or unabsorbed on surface. Based on the values of exponent "n" (n-value > 0.45) obtained from korsmeyer-Peppas model; drug release from NPs followed non-fickian anomalous mechanism predominantly diffusion, erosion and polymer relaxation [29]. Our drug delivery system encapsulated high percentage of drugs i.e. 91.52±3.41% of BCT and 89.24±4.07% of HSP which justified negligible amount of drug loss during preparation of NPs.

We next studied the effect of co-delivery on *in vitro* efficacy of BCT. The cytotoxicity study demonstrated that BCT and HSP co-loaded NPs were more cytotoxic than BCT plus HSP at equivalent concentrations. Additionally, sustained release of drug inside tumor cells could maintain effective drug concentration for longer duration causing lower CC_{50} value. Cell uptake study showed significantly higher accumulation of drugs inside cancer cells by co-loaded NPs which may lead to higher cytotoxicity against PC-3 cells. Further to support our hypothesis apoptotic assays were performed. Annexin-V FITC apoptotic assay showed that the drug co-loaded NPs were more apoptotic than BCT and BCT plus HSP at equivalent concentrations. Whereas blank NPs did not cause significant apoptosis thus proving lack of initiation of any biochemical event that lead to cell death. Co-loaded NPs substantiated more no. of cells at late apoptotic region while reducing no. of cells at necrotic region **(Figure S1)**. Additionally, DAPI apoptotic assay was also performed. As evident from **Figure 3.** Due to the low permeability of DAPI to normal cells, the treatment group that received blank NPs didn't show any florescence. But for the apoptotic cells, the permeability was improved and eventually it stained the apoptotic nuclei. So, the increased strength of blue fluorescence in the treatment groups BCT plus HSP and PCL-BCT-HSP-CS NPs confirmed the more number of apoptotic cells. This enhanced apoptosis by co-loaded NPs can be attributed to inhibition of anti-apoptotic pathways [30]. S. *et. al* reported that BCT blocks the ability of G1 to S phase transformation as it requires a number of chronological events in G1 phase for DNA replication to enter in to S phase [31]. Drug loaded NPs confirmed not only higher G1-S phase cell cycle arrest but also accounted for higher apoptosis which may be correlated with the apoptotic assay. HSP alone at test concentrations did not show much inhibition of cell cycle kinetics but its physical combination with BCT

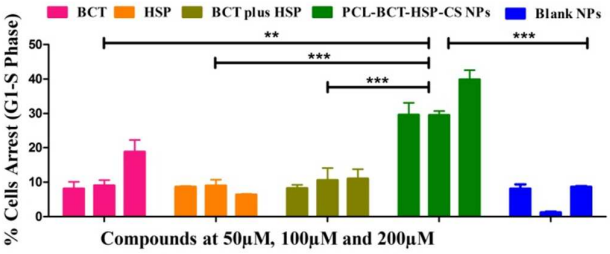

Figure 4. Representation of percent cell cycle arrest at G1-S phase by BCT, HSP, BCT plus HSP, PCL-BCT-HSP-CS NPs and blank NPs. Data are represented as mean ± SD at 50µM, 100µM, and 200µM.

caused G2-M phase arrest. As shown in **Figure 4**; statistically significant difference ($P < 0.05$) relating G1-S phase cell cycle arrest was found between BCT, HSP, BCT plus HSP and PCL-BCT-HSP-CS NPs. Therefore, HSP was supposed to transform cell cycle kinetics. When HSP was co-encapsulated with BCT it appeared that cell cycle arrest occurs at G1-S phase and percentage of cells that were transforming to necrosis were decreased. Therefore it is believed that HSP protects cells from necrosis and was also responsible for enhanced G1-S phase arrest.

In recent years, mitochondrial membrane potential disruption was widely studied for mitochondrial mediated apoptosis [32]. Therefore we also carried out determination of membrane potential disruption as supported pathway leading to apoptosis. In this study, JC-1 staining demonstrated that PCL-BCT-HSP-CS NPs and BCT plus HSP showed more mitochondrial membrane potential loss in contrast to BCT and HSP. Unlike, blank NPs did not show disruption of mitochondrial membrane potential. Further, it was explicated that the apoptosis due to blank NPs is merely due to the G1-S phase cell cycle arrest and blank NPs didn't cause any change in the mitochondrial membrane potential. It has already been reported that HSP showed apoptosis by cell cycle arrest and mitochondrial membrane depolarization through increased expression of caspases in SiHa cells [33]. Recent reports points out that HSP induce apoptosis in MCF-7 cells by generation of cytosolic reactive oxygen species [34]. Therefore it is understood that HSP causes increase in BCT mediated apoptosis via induction of intrinsic mitochondrial apoptotic caspases. These findings suggested that the improvement in apoptotic potential is mediated by co-delivery of BCT and HSP which might be due to the enhanced mitochondrial disruption and cell cycle arrest. Therefore it is necessary to retain structural integrity of HSP in NPs. The structural intactness of HSP was confirmed by DPPH colorimetric assay as no significant difference ($P > 0.05$) between % scavenging activity of HSP as a free drug and in co-loaded NPs was observed **(Figure S2)**.

An ideal nanocarrier should enhance oral bioavailability by increasing solubility and intestinal permeability of hydrophobic drugs. Pharmacokinetic study showed that drug loaded NPs displayed significantly higher plasma level of BCT ($P < 0.001$) and HSP ($P < 0.05$) in comparison to aqueous suspension (BCT plus HSP) at equivalent dose of 20mg/kg after oral administration with subsequent rise in Cmax of both drugs. This increase in Cmax and AUC0-t can be attributed to several factors; (i) Mucoadhesive nature of CS increased the intestinal residence time of NPs [35], (ii) CS has ability to open intestinal tight junctions therefore increased paracelluar transport of drugs, (iii) Increased transport of NPs via transcellular pathway likely by M-cells of peyer's patches [36], (iv) Increase in solubility of drugs. **Figure 1B** shows presumed mechanism of paracellular and transcellular transport of drugs from PCL-BCT-HSP-CS NPs from gut lumen to systemic circulation. However, like most of the flavonoids HSP is effluxed to gut lumen through ATP binding cassettes (ABC) transporters [37] and recently it was indentified that anti-androgens like BCT inhibit ABC efflux [13].This may contribute to increase in intestinal absorption of HSP. The decrease in Tmax may be co-related with increase in solubility of BCT, faster dissolution and gastro-intestinal absorption. NPs may result in concentration dependent and sustained release of drug that will be accounted for longer $t_{1/2}$ than that of aqueous suspension. This interpretation appropriately articulates 1.46 fold and 4.16 fold increase in AUC0-t, and 1.42 fold and 3.79 fold increase in Cmax of BCT and HSP, respectively. Increased bioavailability of BCT and HSP was also reported by many authors [38-40]. Tissue distribution studies of BCT and HSP in NPs were found to be different from that of aqueous suspension. Liver and kidney were the major organs of distribution for both treatment groups. Based on AUC0-t obtained after NPs administration, it was demonstrated that more amount of drugs was accumulated in all tissues (BCT and HSP) except HSP accumulation in intestine and kidney. This may be related to the rapid absorption of HSP from intestine and lower renal elimination. Spleen was being minor organ for drug distribution of BCT suggesting fewer phagocytic uptakes and rapid clearance from mononuclear phagocytes [41]. Minimal pulmonary infiltration can be accountable for low levels of HSP in lungs. Higher tissue to plasma AUC0-t ratio (T/P values) of drugs after NPs administration may be associated with larger disposition of drugs which were largely dependent on properties of NPs. One of the major concern in BCT therapy is its hepatotoxicity. Therefore, 3.59 fold increase ($P < 0.001$) in hepatic levels of HSP is considered important to encounter oxidative stress. Study results explained that particle size and zeta potential influenced the intestinal retention, permeation and cellular uptake by tissues. The increased *in vitro* anti-cancer activity is likely due to the co-delivery of HSP with BCT in NPs.

3. Results

3.1 Solubility studies

Solubility of pure BCT was observed as 0.003mg/mL and it increased 3.6 times for plain precipitated BCT i.e. 0.011mg/mL. Solubility of BCT in NPs was found to be 0.185mg/mL which was 61.66 and 16.81 times higher as compared to BCT and plain precipitated BCT, respectively. The solubility of free HSP was found to be 0.195mg/mL and in NPs it increased 6.75 folds to 1.317mg/mL.

Surfactant type	0.125% v/v			0.250% v/v		
	Average Particle Size, nm	Zeta Potential, mV	PDI	Average Particle Size, nm	Zeta Potential, mV	PDI
PF-127	133.7±20.9	-8.62±1.42	0.686±0.101	152±26.0	-5.17±4.71	0.513±0.042
PVA	340±17.2	-11.43±3.19	0.156±0.076	545±27.8	-6.44±1.17	0.269±0.076
PF-68	175±23.7	-13.71±2.16	0.349±0.053	223±18.1	-9.46±1.92	0.358±0.49
Tween-80	210±11.4	-9.46±2.44	0.295±0.095	167±13.8	-18.4±2.13	0.146±0.081

Table I. Effect of type and concentration of surfactant on particle size (nm), zeta potential (mV) and poly dispersity index (PDI) of NPs.

3.2 Effect of surfactant on particle size and zeta potential

Surfactant plays an important role in reducing interfacial tension and prevents aggregation of particles. Effect of surfactant type and its concentration on particle size and zeta potential was evaluated. Non ionic surfactants PF-127, PVA, PF-68 and T-80 were evaluated at two concentrations i.e. 0.125% v/v and 0.250% v/v. PF-127, PVA and PF-68 resulted in larger particle size or high polydispersity index (PDI). Most optimum particle size (167±13.8nm) and zeta potential (-18.4±2.13mV) for PCL-BCT NPs was obtained by using 0.25%v/v T-80 as surfactant **(Table I)**.

3.3 Nanoparticles Characterization and Stability Studies

Particle size and zeta potential of PCL-BCT-HSP-CS NPs was changed from 281±13.7nm and +12.10±1.11mV to 315±25.9nm and +11.91±1.71mV at refrigerated conditions. Whereas, at room temperature it was changed to 355±21.4nm and 12.80±3.06mV **(Figure S3)**. It was found that there was no significant change ($P > 0.05$) in particle size and zeta potential after the stipulated period as compared to initial values. Furthermore, change in mean particle size was less prominent at refrigerated conditions.

3.4 Drug Release, Encapsulation Efficiency and Drug Release Kinetics

Percent cumulative drug release was plotted against time to predict drug release behavior from NPs and compared with aqueous suspension of drugs **(Figure 5)**. Both NPs and aqueous suspension did not show initial burst release in SGF (less than 8% drugs were released). However, in SIF NPs showed higher percent cumulative drug release for BCT and HSP i.e. and 50.12±3.94% in comparison to aqueous suspension i.e. 18.89±1.34% and 44.72±4.23%, respectively after 24hr. Further in PBS pH 7.4, aqueous suspension didn't show remarkable release after 72hr, whereas NPs confirmed 58.83±4.29% and 81.74±11.32% cumulative release for BCT and HSP respectively. Our drug delivery system was effectively loaded and showed high incorporation efficiency for both BCT (91.52±3.41%) and HSP (89.24±4.07%). Drug release from NPs exhibited high correlation coefficient with korsmeyer-Peppas release kinetic model **(Table SI)**. The model with high correlation coefficient for BCT (R^2; 0.9872) and HSP (R^2; 0.9982) was assumed to be the suitable model demonstrating mechanism of release.

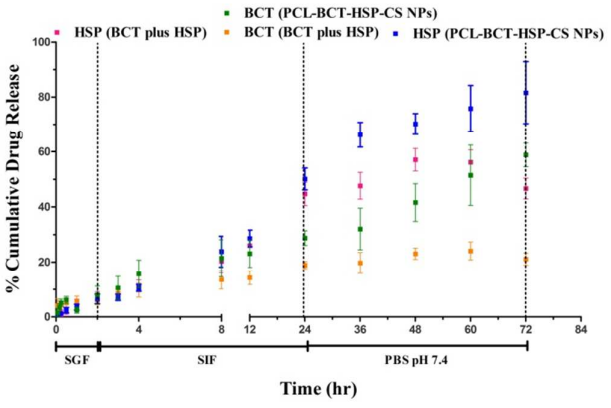

Figure 5. Percent cumulative drug release profile of BCT and HSP from aqueous suspension (BCT plus HSP) and PCL-BCT-HSP-CS NPs. Data are represented as Mean ± SD (n=3).

3.5 In vitro Activity Assessment Assays

3.5.1 Cell Cytotoxicity Assay

The CC_{50} of PCL-BCT-HSP-CS NPs was found to be 22.27µM which is 3.00 fold lower in comparison to BCT plus HSP (66.38µM). The CC_{50} obtained for BCT and HSP was 88.17µM and 959.47µM, respectively. After 24hr of incubation, BCT and HSP combination in free form and in PCL-BCT-HSP-CS-NPs showed significantly higher cytotoxicity as compared to BCT ($P < 0.05$) and HSP ($P < 0.01$) alone. Whereas, insignificant difference ($P > 0.05$) was present between BCT plus HSP and PCL-BCT-HSP-CS NPs. The blank NPs exhibited almost negligible cytotoxicity (CC_{50}: 2532 µM) proving the safety of the excipients used in the formulations **(Figure 6A)**. The percent cell viability after 48hr of incubation has been shown in **Figure S4.**

3.5.2 Cell Uptake Study

In vitro cell uptake studies were performed in PC-3 cells using HPLC. PC-3 cells treated with co-loaded NPs 2.00 ($P < 0.05$) fold

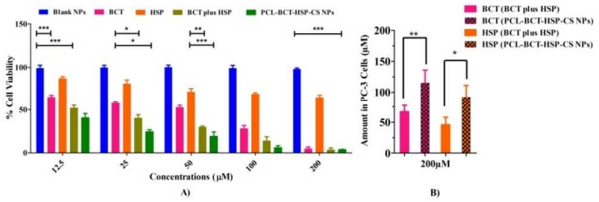

Figure 6A. Representative percent cell viability of PC-3 cells after incubation for 24hr with BCT, HSP, BCT plus HSP, PCL-BCT-HSP-CS NPs, and Blank NPs when treated with 12.5µM, 25µM, 50µM, 100µM and 200µM. **(6B)** Representation of quantitative uptake of drugs from co-loaded NPs compared with free drugs. Estimation shows higher amount of drugs present in PC-3 cells treated with NPs in comparison to free drugs. Data are represented as Mean ± SEM (n=3).

increase in amount of BCT and HSP present in cells in comparison to free drugs **(Figure 6B)**.

3.5.3 Apoptosis

As indicated in **Figure S1**; both BCT (33.54% - 40.03%) and HSP (11.16 - 16.92%) induced cell necrosis in concentration dependent manner. However, HSP at higher concentration (200µM) leads to late apoptosis (28.93%). PCL-BCT-HSP-CS NPs caused recruitment of more number of cells to both PI and annexin-V FITC positive region as compared to BCT plus HSP at identical concentrations. Drug loaded NPs resulted in increased number of cells in late apoptotic and necrotic region. Study demonstrated that when cells were treated with blank NPs only 2.84% cells were stained with PI, 11.23% cells were stained with annexin-V FITC where as only 8.63% cells were both PI and annexin-V FITC positive at higher particle concentration.

As for the DAPI apoptotic assay (**Figure 3)**, the cells that were treated with blank NPs didn't show blue fluorescence. However, BCT showed blue fluorescence and comparatively less fluorescence was observed by HSP group. High fluorescence was visualised in the groups that received combination of BCT and HSP as free drugs or in PCL-BCT-HSP-CS NPs. Also, the number of nuclei that were stained with DAPI has increased which indicated the increase in extent of apoptosis.

3.5.4 Nanoparticles Enhanced G1-S Phase Cell Cycle Arrest

Both BCT and HSP were known to modulate cell cycle kinetics. As shown in **Figure S5**; BCT brought G1-S phase cell cycle arrest in concentration dependent manner i.e. 18.77% cells at 200 µM. But HSP did affect less on cell cycle kinetics at the test concentrations. PCL-BCT-HSP-CS NPs leads to significant higher ($P < 0.001$) G1-S phase arrest as compared to BCT plus HSP at identical concentrations. co-loaded NPs caused 39.85% of cells to G1-S phase arrest at 200µM which was much higher than their physical combination. BCT plus HSP also caused cell cycle arrest at G2-M phase but co-loaded NPs arrested cells at G1-S phase thus limiting their number at G2-M phase. Blank NPs demonstrated that large number of cells (> 78.00 %) remained at G0-G1 phase at all test concentrations.

3.5.5 Mitochondrial Membrane Depolarization Responsible for Apoptosis

In healthy cells with high membrane potential J-aggregates are formed and emits intense red fluorescence. Whereas, apoptotic cells with low membrane potential emits green fluorescence [42]. BCT, HSP, BCT plus HSP and co-loaded NPs confirmed increase in mitochondrial membrane depolarization in concentration dependent manner in PC-3 cells **(Figure 7)**. BCT plus HSP and PCL-BCT-HSP-CS NPs showed 1.46 times and 2.06 times more membrane depolarization at 200µM than free BCT. Co-loaded NPs showed high membrane depolarization i.e. 45.12%, 70.41%, 85.91% at 50µM, 100µM, 200µM in comparison to BCT plus HSP at equivalent concentrations, respectively. The alteration in the mitochondrial membrane potential caused by PCL-BCT-HSP-CS NPs was significantly different by the change due to BCT ($P < 0.05$), HSP ($P < 0.01$) and their combination in free form ($P < 0.01$). Significant

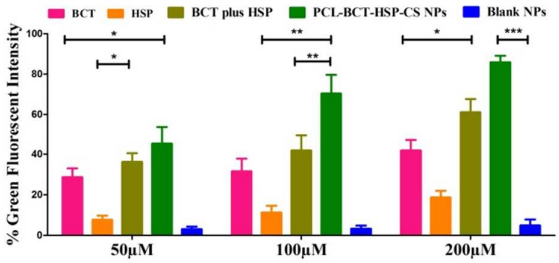

Figure 7. Percent green fluorescent intensity when PC-3 cells were treated by BCT, HSP, BCT plus HSP, PCL-BCT-HSP-CS NPs and blank NPs at 50µM, 100µM and 200µM. Data are represented as Mean ± SD (n=3).

difference ($P < 0.05$) was also present between BCT plus HSP and treatment by individual free drugs. HSP also displayed gradient increase in membrane depolarization i.e. 7.77%, 11.28%, 18.79% at 50µM, 100 µM, 200µM whereas blank NPs showed negligible change in membrane depolarization as compared to control (only 4.98% at 200µM) **(Figure S6)**.

3.6 Thermal Analysis Confirmed Polymorphic Behavior of Bicalutamide

TGA showed change in percent weight loss curve of plain precipitated BCT as compared to pure BCT with respect to temperature. The curve was slightly shifted to left side indicating the decrease in temperature for maximum weight loss. But in both curves, transitions with onset temperature of about 194.13°C (19.81mW) and 195.11°C (11.12mW) are related to melting point (endothermic peak) of BCT and plain precipitated BCT, respectively. None of the endothermic peak was due to the weight loss as indicated by TGA study. The DSC thermogram of physical combination of PCL, CS, BCT and HSP displayed that endothermic peaks of BCT (194.10°C) and HSP (226.24°C) were retained in mixture.

3.7 Anti-oxidant Potential of HSP Retained in NPs

Anti-oxidant potential of BCT, HSP, and HSP plus BCT (1:1), and PCL-BCT-HSP-CS NPs was assessed by DPPH colorimetric assay. HSP showed strong % scavenging activity (89.70±5.11%) and anti-oxidant potential of HSP was retained ($P > 0.05$) in BCT plus HSP (1:1) and PCL-BCT-HSP-CS NPs. On the other hand BCT showed little (8.09±3.26%) scavenging activity.

3.8 Oral Pharmacokinetics and Tissue Distribution

3.8.1 PCL-BCT-HSP-CS NPs Enhanced Oral Bioavailability of BCT and HSP

The effect of kinetic solubility, *in vitro* drug release and on oral bioavailability was studied. The plasma concentration-time profile of drugs in NPs and its comparison with aqueous suspension of BCT plus HSP has been plotted in **Figure 8A & 8B**. The profiles were subjected into non-compartmental analysis. The study showed that the pharmacokinetic profile of BCT and HSP have improved in PCL-BCT-HSP-CS NPs as compared to aqueous suspension (BCT plus HSP). Also, PCL-BCT-HSP-CS NPs resulted in more plasma concentration of both drugs at each time interval than BCT plus HSP aqueous suspension. The area under curve (AUC) (hr ng mL^{-1}) for BCT and HSP in case of NPs (AUC_{0-t} BCT; 227537.50±2324.17, AUC_{0-}

Pharmacokinetic Parameters	BCT (PCL-BCT-HSP-CS) NPs	Aqueous Suspension BCT (BCT plus HSP)	HSP (PCL-BCT-HSP-CS) NPs	Aqueous Suspension HSP (BCT plus HSP)
	Mean ± SEM	Mean ± SEM	Mean ± SEM	Mean ± SEM
AUC_{0-t} (hr ng mL^{-1})	227537.50±2324.17***	160374.32±4566.85	154.75±32.57	87.56±13.91
$AUC_{0-\infty}$(hr ng mL^{-1})	239927.87±3574.89***	163863.30±5647.09	561.93±115.97*	135.02±24.15
C_{max} (ng mL^{-1})	6073±614.81*	4270.59±98.29	50.85±13.67	13.4±3.43
T_{max} (hr)	8±0.1***	12±0.16	0.5±0.13	0.51±0.10
$t_{1/2}$ (hr)	39.99±4.6*	23.46±3	4.23±0.78	3.54±0.85

Table II. Pharmacokinetic parameters of BCT and HSP from PCL-BCT-HSP-CS NPs compared with aqueous suspension (BCT plus HSP) at an oral dose of 20mg/kg. Data are represented as Mean ± SEM (n=3).

$_{\infty}$BCT; 239927.87±3574.89 and AUC_{0-t}HSP; 154.75±32.57, $AUC_{0-\infty}$HSP; 561.93±115.97) was significantly higher than aqueous suspension of BCT plus HSP (AUC_{0-t}BCT; 160374.32±4566.85,$AUC_{0-\infty}$BCT; 63863.30±5647.09 and AUC_{0-t} HSP; 87.56±13.91, $AUC_{0-\infty}$HSP; 135.02±24.15). The peak plasma concentration (C_{max}) (ng mL^{-1}) reported for BCT at T_{max}; ±0.1 hr and HSP at T_{max}; 0.5±0.13 hr (C_{max}BCT; 6073±614.81 and C_{max}HSP; 50.85±13.67) was also higher than aqueous suspension (C_{max}BCT; 4270.59±98.29 and C_{max}HSP; 13.4±3.43).

Other major features of plasma concentration-time profile include prolongation of half life (hr) for BCT ($t_{1/2}$; 39.99±4.6) and HSP ($t_{1/2}$; 4.23±0.78) in comparison to aqueous suspension ($t_{1/2}$BCT; 23.46±3 and $t_{1/2}$HSP; 3.54±0.85). **Table II.** illustrates pharmacokinetic parameters of BCT and HSP from PCL-BCT-HSP-CS NPs and aqueous suspension.

3.8.2 Tissue Distribution

Mean concentration–time profile of BCT and HSP in various tissues has been shown in **Figure 9A & 9B**; and related pharmacokinetic parameters were elaborated in **Table III**. In animals treated with PCL-BCT-HSP-CS NPs, AUC_{0-t} of BCT has increased as compared to BCT plus HSP aqueous suspension but significant difference was only present in the intestine. The T_{max} for BCT has reduced in each tissue except heart and kidney where it was prolonged to 4.0hr and 8.0hr, respectively. In animals treated with NPs amount of BCT and HSP present in tissues after 24hr of administration of was higher than aqueous suspension. Co-loaded NPs has displayed significant higher ($P < 0.001$) AUC_{0-t} of HSP in liver and significant lower ($P < 0.01$) AUC_{0-t} in intestine. The time to reach C_{max} of HSP following NPs administration has been increased in spleen and decreased in heart and lungs. The AUC_{0-t} of drugs in different organs was represented in **Figure S7.**

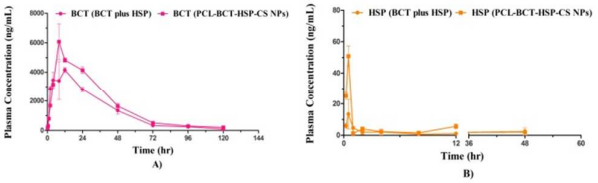

Figure 8. Representative plasma concentration-time profile of A) BCT and B) HSP from PCL-BCT-HSP-CS NPs at 20mg/kg in SD male rats compared with equivalent dose of BCT plus HSP aqueous suspension after oral administration. Data are represented as Mean ± SEM (n=3).

4. Experimental

4.1 Materials, Cell lines and Animals

Hesperetin, Chitosan, Bicalutamide, 2,2-diphenyl-1-picryl-hydrazyl-hydrate (DPPH), RPMI-1640, Sodium bicarbonate, 3-(4,5-Dimethylthiazol-2-Yl)-2,5-Diphenyltetrazolium Bromide (MTT), Propidium Iodide (PI), 4,6-diamidino-2-phenylindole-2-HCl (DAPI), Ribonuclease A, Trypsin and Tween-80 were purchased from Sigma-Aldrich (USA, St. Louis). Apoptosis detection kit, Fetal Bovine Serum (FBS), PBS tablets, Ethanol, HPLC grade Acetonitrile (ACN) and JC-1 dye (5,5',6,6'-tetrachloro - 1, 1', 3, 3' - tetraethylbenzimidazolylcarbocyanine - iodide), were obtained from Merck India Ltd. (Mumbai, India). Beparine, a heparin sodium injection I.P. with 25,000 IU in 5mL was obtained from Biological E. Limited (Hyderabad, India). Glacial acetic acid extrapure was purchased from Sisco Research Laboratories Pvt. Ltd., Mumbai. Polycaprolactone (PCL), powdered (M.Wt. 50,000) was purchased from Polyscience, Inc. N,N-dimethyl formamide, dimethyl-sulphoxide was procured from spectrochem Pvt. Ltd. Mumbai.

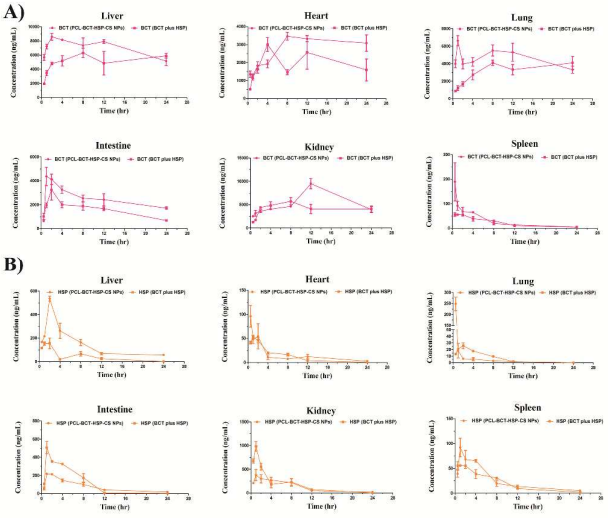

Figure 9. Mean concentration–time profile of **A)** BCT and **B)** HSP in various tissue from PCL-BCT-HSP-CS NPs at 20mg/kg in SD male rats compared with equivalent dose of BCT plus HSP aqueous suspension after oral administration. Data are represented as Mean ± SEM (n=3).

Organ	BCT (PCL-BCT-HSP-CS NPs) AUC $_{0-t}$ (Mean ± SD) (hr ng mL^{-1})	BCT (BCT plus HSP) AUC $_{0-t}$ (Mean ± SD) (hr ng mL^{-1})	T/P AUC 0-t Ratio# BCT (PCL-BCT-HSP-CS NPs)	T/P AUC 0-t Ratio# BCT (BCT plus HSP)
Liver	169188.8 ± 11840.15	145958.0 ± 0745.53	2.14	1.25
Heart	69084.0 ± 6050.07	48550.5 ± 13275.62	1.76	1.03
Lung	109915.5 ± 16115.61	79614.3 ± 12660.7	1.39	0.79
Intestine	59406.3 ± 7834.49	37789.1 ± 5468.31	0.87	0.48
Kidney	139334.9 ± 14434.34	103066.9 ± 7732.65	0.01	0.01
Spleen	678.6 ± 141.36	505.2 ± 50.53	0.75	0.38
Organ	**HSP (PCL-BCT-HSP-CS NPs) AUC $_{0-t}$ (Mean ± SD) (hr ng mL^{-1})**	**HSP (BCT plus HSP) AUC $_{0-t}$ (Mean ± SD) (hr ng mL^{-1})**	**T/P AUC $_{0-t}$ Ratio# HSP (PCL-BCT-HSP-CS NPs)**	**T/P AUC $_{0-t}$ Ratio# HSP (BCT plus HSP)**
Liver	3373.9 ± 425.62	937.86 ± 246.89	83.82	9.27
Heart	344.863±118.48	292.32 ± 34.59	8.57	2.89
Lung	188.4±49.39	166.4±20.09	4.68	1.64
Intestine	1779.5±169.95	2703.278.65	44.22	26.74
Kidney	2979.6 ± 870.46	3950.2 ± 744.15	74.03	39.07
Spleen	603.6 ± 106.0	477.8 ± 54.40	15.00	4.72

Table III. Pharmacokinetic parameters in A) BCT, and B) HSP of different organs from PCL-BCT-HSP-CS NPs at 20mg/kg in SD male rats compared with aqueous suspension (BCT plus HSP) at an oral dose of 20mg/kg. Data are represented as Mean ± SEM (n=3). # T/P denoting tissue/plasma AUC 0-t Ratio

HPLC grade water was obtained from Millipore Elix water purification system (Millipore India Pvt. Ltd., New Delhi, India). Other solvents used were of analytical grade. PC-3 cells androgen independent prostate cancer cell lines) were procured from cell library of CSIR-CDRI. Male SD rats (120-150gm) were procured from the National Laboratory Animal Centre of CSIR-CDRI, Lucknow, India and with necessary approval vide IAEC/2015/18 dated 15-04-2015 of the Institute Animal Ethical Committee, the experiments were carried out. The animals were allowed ad libitum access to water and rodent chow throughout the study.

4.2 Methods

4.2.1 Preparation of Nanoparticles and determination of Encapsulation Efficiency

The NPs containing BCT and HSP were prepared by anti-solvent precipitation followed by ion-gelation method as per our previous paper with slight modification [43]. Encapsulation efficiency (EE) was expressed as percentage of drug present in NPs relative to initial amount of drug used for preparation [44].

4.2.2 In vitro Drug Release and Release Kinetics

In vitro drug release studies of aqueous suspension (BCT plus HSP) and PCL-BCT-HSP-CS NPs were performed in simulated gastric fluid at pH 1.2 (SIF) for 2hr, simulated intestinal fluid (SIF) at pH 6.8 up to 24hr and in phosphate buffer saline (PBS) pH 7.4 for remaining period of study using dialysis membrane (Sigma-Aldrich, Molecular weight cut off 12,000–14,000 Dalton) method [45]. The samples of drug release were then analyzed by HPLC .

Different release models like zero order ($A = k_0t$), first order ($\log UA = k_1t/2.303$), Higuchi ($A = K_2\sqrt{t}$) and korsmeyer-Peppas ($A = k_3tn$) were applied to assess the mechanism of drug release, where K_0, K_1, K_2, and K_3 describes zero order, first order, Higuchi and Korsmeyer-Peppas rate constants. Here, A and UA are the percent amount of drug released and unreleased at time t; n is the exponent that describes particular release diffusion mechanism [46].

4.2.3 Characterization of Nanoparticles and Stability Studies

The hydrodynamic diameter and particle size distribution of NPs was measured by photon correlation spectroscopy using Malvern Zetasizer Nano ZS90 (Malvern Instruments, UK). Zeta potential was assessed by measuring electrophoretic mobility of the particles employing a laser based multiple angle electrophoresis analyzer. The shape and surface morphology of BCT, plain precipitated BCT, and PCL-BCT NPs and PCL-BCT-HSP-CS NPs were visualized by scanning electron microscopy (SEM) (JSM-6390LV (JEOL, Japan). The freeze dried PCL-BCT-HSP-CS NPs were stored at refrigerated conditions (4±0.5^{o}C) and room temperature (25±0.5^{o}C) for 3 months to predict their physical stability.

4.3 In Vitro Efficacy Assessment Studies

4.3.1 Cell Culture

PC-3 cells (cultured in 25cm^2 tissue culture flasks and maintained in a 5% CO_2 atmosphere at 37°C) were used for all in vitro activity studies. The cell medium was supplemented with Roswell Park Memorial Institute medium (RPMI)-1640 modified with L-glutamine, phenol red and sodium bicarbonate (2.0g/1000mL), and 10% fetal bovine serum (FBS). PC-3 cells at a cell density of 1x10^5 cells per well were incubated at 37^{o}C for 24hr in 96 well plates or 6-well plates and cells were harvested by trypsinization.

4.3.2 Cytotoxicity Assay

It is usually done by MTT assay [47] and expressed as CC_{50}, the concentration which is toxic to 50% of the cells. PC-3 cells

were incubated with different concentrations in culture media for 24hr and 48hr. Subsequently, 5µL MTT (5mg/mL) was added to each well and incubated for another 3hr at 37°C. It was followed by replacement of culture media by dimethyl-sulphoxide (100µL) to dissolve formazan crystal [48]. A graph was constructed between percent cell viability and test concentrations of different compounds and the CC_{50} values were calculated by non-linear regression model [48].

4.3.3 Cell Uptake Study

HPLC was utilized to investigate cellular uptake of co-loaded NPs and compared with free drugs. PC-3 cells were incubated at 200 µM for 24hr. The cells were harvested and then washed three times with PBS pH 7.4 to remove surface adhered drugs. After that ACN (2mL) was added, sonicated for 5min to extract out drugs and filtered. Filtrate was then analyzed by HPLC.

4.3.4 Apoptotic Assay

Detection of apoptosis was done using annexin V-FITC assay and DAPI apoptotic assay according to the manufacturer's protocol. For annexin V-FITC assay, after 24hr of treatment, the cells were washed and suspended in 500µL of PBS. Then cells were stained with 1.25µL of annexin V-FITC and 10µL of binding buffer, and incubated in dark for 15min at room temperature. Following, 10µL PI was added and samples were kept on ice. Samples were analyzed by BD FACS Calibur flow cytometer (BD Bioscience FACS Aria, Germany) equipped with Cell Quest Pro software. For DAPI staining, PC-3 cells were incubated on to sterile cover-slips in a 6-well plate for 24hr. After treatment with different groups at 100µM concentration for 24hr, the cells were washed with PBS three times. It was followed by staining with 1mL of PBS containing DAPI (1µg/mL) for 10min at 37°C. The cells were again washed with PBS three times and fixed in 1mL 4 % formaldehyde solution for 20 min. After washing with PBS, cover-slips were mounted (cell-side down) on slides using glycerol: PBS (9:1) as mounting media. Apoptotic cells were visualized with a fluorescent microscope (Nikon Eclipse TS 100) equipped with NIS-Element F.4.00.00 software at an excitation wavelength of 350nm.

4.3.5 Cell Cycle Distribution

For cell cycle distribution study, PI was used as a fluorescent marker. All adhering and floating cells were harvested and transferred to sterile micro-centrifuge tubes [18]. The cells were then washed with cold PBS and fixed in PBS: ethanol (1:9) at 4°C for overnight. Next day cells were centrifuged at 1,000rpm for 5min, then suspended in 500µL of cold PBS with Ribonuclease A (100µg/mL) and Triton-X (1%) for 30min at 37±0.5°C. After that cells were stained by PI (50µg/mL) for 30min. The samples were immediately analyzed using BD FACS Calibur flow cytometer.

4.3.6 Mitochondrial Membrane Potential

To predict pathway involved in apoptosis, mitochondrial membrane potential was measured utilizing JC-1 dye (Molecular Probes, Eugene, OR). Changes in the membrane potential are presumed to be due to the opening of the mitochondrial permeability transition pore (MPTP), allowing passage of ions and small molecules [49]. After 24hr of incubation; PC-3 cells were harvested and stained with 5µL of JC-1 dye (10µg/mL) for 30min at 37°C. All samples were washed thrice with PBS to remove unattached dye. Finally the cells were suspended in 500µL PBS and loss in mitochondrial membrane potential was measured by flow cytometer (BD FACS Calibur).

4.4 Anti-oxidant Assay

There are chances of structural integrity loss and thus the anti-oxidant potential of HSP during preparation of NPs. Antioxidant activity of freeze dried PCL-BCT-HSP-CS NPs was evaluated by DPPH assay followed by the method reported in the literature [50]. Briefly, working standards solutions (100µM) of free drugs; BCT, HSP and BCT plus HSP (1:1) and freeze-dried blank NPs were prepared in methanol. To 40µL solution of free drugs or drugs extracted from NPs, 100µL methanolic solution of DPPH (200µM) reagent was added. The reaction mixture was incubated in dark at room temperature for 1hr, and the absorbance (A) was recorded at 517nm using microplate UV spectrophotometer (BioTek, USA). The radical scavenging ability was calculated as:

$$\%\text{Scavenging Effect} = [(A_c - A_s)*100]/A_c$$

Where A_c is the absorbance of the control and A_s is the absorbance in the presence of samples or standards.

4.5 Thermogravimetric Analysis (TGA) and Differential scanning Calorimetry (DSC)

TGA and DSC were performed by Perkin Elmer Thermogravimetric Analyzer equipped with PYRIS version 8.0 software. It has been reported that BCT existed in two polymorphic forms; form I and form II [51]. In our study, TGA was performed to study polymorphic behavior of BCT during preparation of NPs. BCT was precipitated by same method as used for preparation of NPs but only lacking polymers used. Percent weight loss curve was compared and same curve was converted in to heat flow curve (DSC thermogram) to predict endothermic behavior of both samples. Further, DSC thermograms of HSP, PCL, CS and PCL+BCT+HSP+CS were obtained to anticipate the compatibility of excipients with drugs.

4.6 Oral Pharmacokinetics Studies

4.6.1 Instrumentation and Chromatographic Conditions

Chromatographic separation was achieved on a Waters Symmetry-Shield C18 (5µ, 4.6 X 150mm) column, using ACN: 0.1% formic acid (80:20v/v) as the mobile phase. All separations were performed in binary mode at a flow rate of 0.7mL/min and the injection volume was kept at 20µL. Bio-analysis was performed using API 3200 mass spectrometer (Applied Biosystems, Canada) coupled with an electro spray ionization (ESI) source using negative multiple reaction monitoring (MRM) mode. **Figure S8;** shows the MRM Chromatograms of; A) Bicalutamide, B) Hesperetin, C) Topiramate.

4.6.2 Plasma and Tissue Sample Preparation

In vivo oral pharmacokinetic study was carried out in male SD rats (120–150gm). BCT plus HSP in 0.25% sodium CMC aqueous suspension and PCL-BCT-HSP-CS NPs were administered orally at an equivalent dose of 20mg/kg. The blood samples were withdrawn through retro-orbital plexus under light anaesthesia. For tissue distribution study liver, heart, lung, intestine, kidney and spleen were harvested after

cervical dislocation at predefined time intervals and homogenized at 18,000rpm (IKA® T-25 digital Ultra Turax, Germany) after suitable dilution with PBS pH 7.4. Samples were prepared by protein precipitation technique using ACN as an precipitating/extracting solvent. To 50µL each of calibration standard/plasma/tissue homogenate, 150µL of ACN containing internal standard (Topiramate 500ng/mL) was added, vortexed for 5min. and centrifuged at 14,000g for 20min. Following centrifugation, 20µL supernatant was injected into LC-MS/MS system (API 3200) for analysis. Concentration (ng/mL) of analytes in plasma and tissues were calculated from standard curve.

4.6.3 Data Analysis

The data obtained from pharmacokinetic parameters were analyzed statistically using WinNonlin® version 5.1 software. Statistically significant differences were assumed at $P < 0.05$.

4.7 Statistical Analysis

All experiments were conducted in triplicate and data were expressed as mean ± standard deviation. Statistical analysis was performed using GraphPad Prism® version 5.03 software. One way Analysis of Variance was used with Tukey's test for comparison of means and probability values ($P < 0.05$) was considered as statistical significant. Asterisk represents the level of significant difference ($*p < 0.05$, $**p < 0.01$ and $***p < 0.001$).

5. Conclusions

In summary, we have suggested preparation of polymeric nanoparticles (PCL-BCT-HSP-CS NPs) for co-delivery of BCT and HSP using biodegradable polycaprolactone (PCL) and chitosan (CS). The NPs were capable of trouncing complications of low oral bioavailability and solubility of hydrophobic anti-cancer drugs. Co-loaded NPs showed excellent in vitro activity against androgen independent PC-3 cell lines as confirmed by cytotoxicity assay, cell cycle distribution and apoptotic assay in comparison to free BCT. Increased depolarization of mitochondrial membrane would be the responsible for enhanced apoptosis. More importantly, co-loaded NPs may alleviate oxidative stress emerged due to BCT therapy; owing to increase in hepatic levels of HSP. Hence, co-delivery of BCT and HSP in NPs could not only enhance in vitro therapeutic efficacy and bioavailability but toxicity and drug dependency can also be minimized. In view of authors, PCL and CS based BCT and HSP co-delivery system may offer an attractive alternative for enhancing *in vitro* therapeutic efficacy against androgen independent prostate cancer cell lines.

6. Acknowledgements

Financial supports to authors from Council of Scientific and Industrial Research (CSIR) New Delhi, India, are gratefully acknowledged. We also acknowledge the help of Mr. A. L. Vishwakarma and Mrs. M. Chaturvedi for the flow cytometry study, from Sophisticated Analytical Instrument Facility; CSIR-CDRI, Lucknow.

7. Notes and References

***Corresponding Author**: Dr. A.K. Dwivedi, PCS-001/11, Pharmaceutics Division, CSIR-Central Drug Research Institute, BS 10/1, Sector 10, Jankipuram Extension, Lucknow-226031, INDIA.
Email: anilcdri@gmail.com, abhishekarya55@gmail.com
CDRI Communication No. 282/2015/AKD

1. D. Ilic, M. M. Neuberger, M. Djulbegovic and P. Dahm, *Cochrane Database Syst Rev*, 2013, 1.
2. R. L. Siegel, K. D. Miller and A. Jemal, *CA: a cancer journal for clinicians*, 2015, 65, 5-29.
3. J. W. Moul, *The Canadian journal of urology*, 2014, 21, 22-27.
4.http://www.fda.gov/Safety/MedWatch/SafetyInformation/Safety-RelatedDrugLabelingChanges/ucm133082.htm, 2015.
5. M. Danquah, F. Li, C. B. Duke III, D. D. Miller and R. I. Mahato, *Pharmaceutical research*, 2009, 26, 2081-2092.
6. B. Xiao, X. Si, M. K. Han, E. Viennois, M. Zhang and D. Merlin, *Journal of Materials Chemistry B*, 2015.
7. A. K. Jain, K. Thanki and S. Jain, *Molecular pharmaceutics*, 2013, 10, 3459-3474.
8. A. R. G. Sivakumar Balasubramanian, Y. Nagaoka, S. Iwai, M. Suzuki, V. Kizhikkilot, Y. Yoshida, T. Maekawa and S. D. Nair, *International journal of nanomedicine*, 2014, 9, 437.
9. H. Parhiz, A. Roohbakhsh, F. Soltani, R. Rezaee and M. Iranshahi, *Phytotherapy Research*, 2015, 29, 323-331.
10. S. Sambantham, M. Radha, A. Paramasivam, B. Anandan, R. Malathi, S. R. Chandra and G. Jayaraman, *Asian Pac J Cancer Prev*, 2013, 14, 4347-4352.
11. V. B. Pokharkar, T. Malhi and L. Mandpe, *Pharmaceutical development and technology*, 2013, 18, 660-666.
12. M. Fathi, J. Varshosaz, M. Mohebbi and F. Shahidi, *Food and Bioprocess Technology*, 2013, 6, 1464-1475.
13. Y. Zhu, C. Liu, C. Armstrong, W. Lou, A. Sandher and A. C. Gao, *Clinical Cancer Research*, 2015, clincanres. 0269.2015.
14. S. Jain, R. Jain, M. Das, A. K. Agrawal, K. Thanki and V. Kushwah, *RSC Advances*, 2014, 4, 29193-29201.
15. X. Deng, M. Cao, J. Zhang, K. Hu, Z. Yin, Z. Zhou, X. Xiao, Y. Yang, W. Sheng and Y. Wu, *Biomaterials*, 2014, 35, 4333-4344.
16. N. R. Patel, A. Rathi, D. Mongayt and V. P. Torchilin, *International journal of pharmaceutics*, 2011, 416, 296-299.
17. W. Scarano, P. de Souza and M. H. Stenzel, *Biomaterials Science*, 2015.
18. K. Sharma, S. Pachauri, K. Khandelwal, H. Ahmad, A. Arya, P. Biala, S. Agrawal, R. Pandey, A. Srivastava and A. Srivastav, *Drug research*, 2015.
19. M. M. Mkandawire, M. Lakatos, A. Springer, A. Clemens, D. Appelhans, U. Krause-Buchholz, W. Pompe, G. Rödel and M. Mkandawire, *Nanoscale*, 2015.
20. T. K. Dash and V. B. Konkimalla, *Journal of Controlled Release*, 2012, 158, 15-33.
21. T. Govender, Y. E. Choonara, P. Kumar, L. C. Du Toit, G. Modi, D. Naidoo and V. Pillay, *Polymers*, 2015, 7, 1145-1176.
22. N. Shrestha, M.-A. Shahbazi, F. Araújo, H. Zhang, E. M. Mäkilä, J. Kauppila, B. Sarmento, J. J. Salonen, J. T. Hirvonen and H. A. Santos, *Biomaterials*, 2014, 35, 7172-7179.
23. G. Loch-Neckel, L. Santos-Bubniak, L. Mazzarino, A. V. Jacques, B. Moccelin, M. C. Santos-Silva and E. Lemos-Senna,

Journal of Pharmaceutical Sciences, 2015, DOI: 10.1002/jps.24548, n/a-n/a.

24. B. Fadeel and D. Boraschi, *Nanotoxicology: Progress toward Nanomedicine*, 2014, 315.

25. A. Z. Wang, R. Langer and O. C. Farokhzad, *Annual review of medicine*, 2012, 63, 185-198.

26. G. L. Perlovich, S. V. Blokhina, N. G. Manin, T. V. Volkova and V. V. Tkachev, *Journal of thermal analysis and calorimetry*, 2013, 111, 655-662.

27. K. Y. Win and S.-S. Feng, *Biomaterials*, 2005, 26, 2713-2722.

28. P. Huang, C. Yang, J. Liu, W. Wang, S. Guo, J. Li, Y. Sun, H. Dong, L. Deng and J. Zhang, *Journal of Materials Chemistry B*, 2014, 2, 4021-4033.

29. A. Jaipal, M. Pandey, A. Abhishek, S. Vinay and S. Charde, *Colloids and Surfaces B: Biointerfaces*, 2013, 111, 644-650.

30. V. K. Pawar, S. B. Panchal, Y. Singh, J. G. Meher, K. Sharma, P. Singh, H. K. Bora, A. Singh, D. Datta and M. K. Chourasia, *Journal of Controlled Release*, 2014, 196, 295-306.

31. S. Murthy, M. Wu, V. U. Bai, Z. Hou, M. Menon, E. R. Barrack, S.-H. Kim and G. Reddy, *PloS one*, 2013, 8.

32. N. M. Schaeublin, L. K. Braydich-Stolle, A. M. Schrand, J. M. Miller, J. Hutchison, J. J. Schlager and S. M. Hussain, *Nanoscale*, 2011, 3, 410-420.

33. A. A. Alshatwi, E. Ramesh, V. Periasamy and P. Subash-Babu, *Fundamental & clinical pharmacology*, 2013, 27, 581-592.

34. S. Palit, S. Kar, G. Sharma and P. K. Das, *Journal of cellular physiology*, 2015, 230, 1729-1739.

35. C. He, L. Yin, C. Tang and C. Yin, *Biomaterials*, 2012, 33, 8569-8578.

36. M.-C. Chen, F.-L. Mi, Z.-X. Liao, C.-W. Hsiao, K. Sonaje, M.-F. Chung, L.-W. Hsu and H.-W. Sung, *Advanced drug delivery reviews*, 2013, 65, 865-879.

37. W. Brand, P. A. van der Wel, M. J. Rein, D. Barron, G. Williamson, P. J. van Bladeren and I. M. Rietjens, *Drug Metabolism and Disposition*, 2008, 36, 1794-1802.

38. A. Chaurasiya, A. K. Singh, S. C. Upadhyay, D. Asati, F. J. Ahmad, R. Mukherjee and R. K. Khar, *Advanced Science Letters*, 2012, 11, 43-52.

39. H. Takumi, H. Nakamura, T. Simizu, R. Harada, T. Kometani, T. Nadamoto, R. Mukai, K. Murota, Y. Kawai and J. Terao, *Food & function*, 2012, 3, 389-398.

40. G. Shete, Y. B. Pawar, K. Thanki, S. Jain and A. K. Bansal, *Molecular pharmaceutics*, 2015, 12, 1158-1170.

41. A. C. Anselmo, V. Gupta, B. J. Zern, D. Pan, M. Zakrewsky, V. Muzykantov and S. Mitragotri, *ACS nano*, 2013, 7, 11129-11137.

42. X. Yan, X. Yang, X. Hao, Q. Ren, J. Gao, Y. Wang, N. Chang, Y. Qiu and G. Song, *Biological trace element research*, 2015, 1-6.

43. A. Arya, K. Khandelwal, A. Singh, H. Ahmad, S. Agrawal, R. Khatik, N. Mittapelly and A. K. Dwivedi, *Journal of chromatographic science*, 2015, bmv042.

44. S. Gadde, O. Even-Or, N. Kamaly, A. Hasija, P. G. Gagnon, K. H. Adusumilli, A. Erakovic, A. K. Pal, X. Q. Zhang and N. Kolishetti, *Advanced healthcare materials*, 2014, 3, 1448-1456.

45. H. Peng, W. Li, F. Ning, L. Yao, M. Luo, X. Zhu, Q. Zhao and H. Xiong, *Journal of agricultural and food chemistry*, 2014, 62, 626-633.

46. C. G. England, M. C. Miller, A. Kuttan, J. O. Trent and H. B. Frieboes, *European Journal of Pharmaceutics and Biopharmaceutics*, 2015, 92, 120-129.

47. M. Zhang, D. Aguilera, C. Das, H. Vasquez, P. Zage, V. Gopalakrishnan and J. Wolff, *Anticancer research*, 2007, 27, 35-38.

48. L. P. Mendes, J. M. F. Delgado, A. D. A. Costa, M. S. Vieira, P. L. Benfica, E. M. Lima and M. C. Valadares, *Toxicology in Vitro*, 2015.

49. E. Gottlieb, S. Armour, M. Harris and C. Thompson, *Cell Death & Differentiation*, 2003, 10, 709-717.

50. R. Erenler, O. Sen, H. Aksit, I. Demirtas, A. S. Yaglioglu, M. Elmastas and İ. Telci, *Journal of the Science of Food and Agriculture*, 2015.

51. D. R. Vega, G. Polla, A. Martinez, E. Mendioroz and M. Reinoso, *International journal of pharmaceutics*, 2007, 328, 112-118.

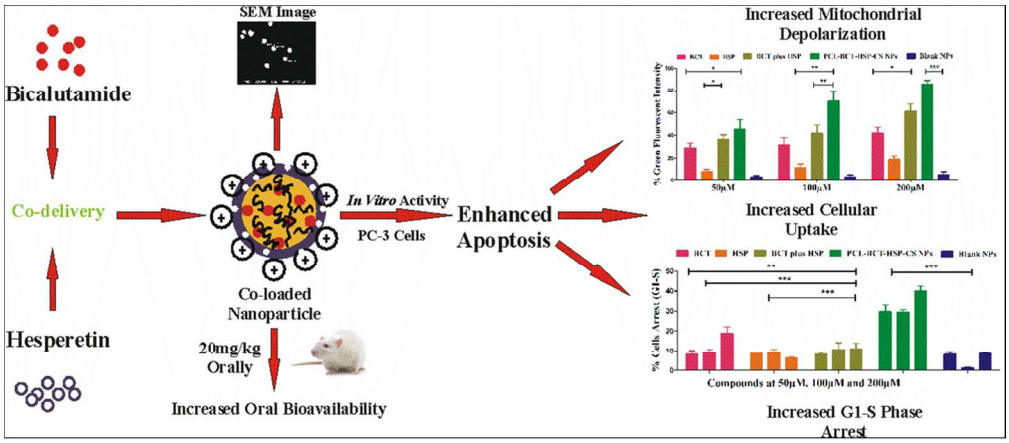

254x110mm (129 x 129 DPI)